Generalized Inversion of Tropical Atmosphere–Ocean (TAO) Data and a Coupled Model of the Tropical Pacific. Part II: The 1995–96 La Niña and 1997–98 El Niño

ANDREW F. BENNETT AND BOON S. CHUA

College of Oceanic and Atmospheric Sciences, Oregon State University, Corvallis, Oregon

D. ED HARRISON AND MICHAEL J. MCPHADEN

NOAA/Pacific Marine Environmental Laboratory, Seattle, Washington

(Manuscript received 10 June 1998, in final form 6 October 1999)

ABSTRACT

The investigation of the consequences of trying to blend tropical Pacific observations from the Tropical Atmosphere–Ocean (TAO) array into the dynamical framework of an intermediate coupled ocean–atmosphere model is continued. In a previous study it was found that the model dynamics, the prior estimates of uncertainty in the observations, and the estimates of the errors in the dynamical equations of the model could not be reconciled with data from the 1994–95 period. The error estimates and the data forced the rejection of the model physics as being unacceptably in error. In this work, data from two periods (1995–96 and 1997–98) were used when the tropical Pacific was in states very different from the previous study. The consequences of increasing the prior error estimates were explored in an effort to find out if it is possible at least to use the intermediate model physics to assist in mapping the observations into fields in a statistically consistent way.

It was found that such a result is possible for the new data periods, with larger prior error assumptions. However, examination of the behavior of the mapped fields indicates that they have no dynamical utility. The model dynamical residuals, that is, the size of the quantity that is left after evaluating all of the terms in each intermediate model equation, dominate the terms themselves. Evidently the intermediate model is not able to add insight into the processes that caused the tropical Pacific to behave as it was observed to, during these time intervals.

The inverse techniques described here together with the relatively dense TAO dataset have made it possible for the unambiguous rejection of the nonlinear intermediate model dynamical system. This is the first time that data have been able to provide such a clear-cut appraisal of simplified dynamics.

1. Introduction

We consider the generalized inversion of Tropical Atmosphere–Ocean (TAO) data and a coupled model of the tropical Pacific. Generalized inversion is the calculation of circulation fields that are weighted least squares best fits simultaneously to TAO data and to the equations of motion of our modified Cane–Zebiak model (Zebiak and Cane 1987). In a previous paper (Bennett et al. 1998, hereinafter B98), we described the model in detail and reported calculations of the simultaneous best fit to the 30-day averaged sea surface temperature (SST), 20°C isotherm depth (Z20), surface winds $\mathbf{u}^a = (u^a, v^a)$, the coupled dynamic, and the initial conditions during the ''smoothing'' interval April 1994–March 1995, (year 1). The western-central equatorial Pacific was warmer than normal and the eastern Pacific nearly normal during the interval. The TAO data reveal an equatorial warm pool that reached a maximum SST anomaly of +2.5°C by November 1994 and disappeared by March 1995. The best-fit circulation fields conformed closely to the TAO data, but left significantly large residuals in the equations of motion, exceeding prior estimates of the residuals based on scale analyses of neglected but numerically resolvable processes. The χ^2 test statistic for the prior covariances exceeded its expected value by 16 standard deviations. This suggests the need to revise the priors, but is only one test. Hence we made two more tests of the identical model and priors, using data for other climatological extremes. The second test involved TAO data for April 1995–March 1996 (year 2), which included a mild La Niña event; the third test involved TAO data for December 1996–May 1998 (year 3), which included one of the major El Niño events of modern times with situations different in character to those of 1994–95. These two new inversions are reported here briefly. We anticipate ourselves by stating

Corresponding author address: Dr. Andrew F. Bennett, College of Oceanic and Atmospheric Sciences, Oregon State University, 104 Ocean Admin. Bldg., Corvallis, OR 97331-5503.
E-mail: bennett@oce.orst.edu

that the same hypothesized covariances are rejected at about the same level of significance as before. Having established that the model, over a wide range of oceanic conditions, cannot be reconciled with the data and our a priori error assumptions, we then explore the effects of weakening these error assumptions. One of the appealing features of the type of inverse study described here is the possibility of such explorations. Of course, it is only sensible to weaken the error assumptions up to the point that respects the most reasonable conservatism concerning the data and the dynamics. Relaxing the error assumptions beyond that point may well yield an inverse solution that meets the constraints, but is not dynamically useful or is not a reasonably accurate ''mapping'' of the observations.

The outline of this paper is as follows. A few details of the model and inverse formulation are given in section 2. Complete details are available in B98. The minimization algorithm is not described as it is highly intricate and fully documented elsewhere (Bennett 1992; Bennett et al. 1996, 1997). The hypothesized dynamical, initial, and data error parameters are restated here for convenience with brief explanations.

Selected results for the inversions for years 2 and 3 are presented in section 3. The significance tests are described in section 4, along with a discussion of the effects of varying the prior covariances. Inverses with revised covariances have not been performed; only the impact on test statistics is estimated. Instead, dynamical term balances for the original inverses are examined in section 5. Our conclusions are presented in section 6.

2. Some details

The ocean model domain is a rectangle on the equatorial β plane with Cartesian coordinates (x, y), in the intervals $x_w = 123.75°\text{E} \le x \le x_e = 84.52°\text{W}$ and $y_s = 29°\text{S} \le y \le y_n = 29°\text{N}$. The atmospheric domain is a circumferential zone on the same plane: $0° \le x \le 360°$ and $y_s \le y \le y_n$. The state variables are the time-dependent fields of oceanic upper or mixed layer velocity $\mathbf{u}^{(1)} = [u^{(1)}, v^{(1)}]$, thickness $\theta^{(1)}$, sea surface temperature T, lower or seasonal thermocline layer velocity $\mathbf{u}^{(2)} = [u^{(2)}, v^{(2)}]$, thickness $\theta^{(2)}$, atmospheric surface wind $\mathbf{u}^a = (u^a, v^a)$, and surface geopotential ϕ^a. All state variables are anomalies with respect to the climatology of Rasmussen and Carpenter (1982). The complete state vector field $\mathbf{U} = \mathbf{U}(\mathbf{x}, t)$ has 10 components:

$$\mathbf{U} = \begin{pmatrix} u^a \\ v^a \\ \phi^a \\ u^{(1)} \\ v^{(1)} \\ \theta^{(1)} \\ T \\ u^{(2)} \\ v^{(2)} \\ \theta^{(2)} \end{pmatrix}. \tag{2.1}$$

The model dynamics are those of Zebiak and Cane (1987), except that all six local accelerations are retained in all six horizontal momentum equations. Thus, all 10 variables are prognostic, and so rigid (no normal flow) boundary conditions may be imposed at x_w, x_e, y_s, and y_n. Horizontal eddy viscosity is included in the oceanic dynamics. No slip holds at x_w, x_e; there is free slip at y_s, y_n. The narrow meridional Munk layers at x_w and x_e are resolved numerically. Divergence dissipation (Talagrand 1972) is also included in the oceanic dynamics. All details may be found in B98.

The data are expressed formally as

$$\mathbf{d} = \mathcal{L}[\mathbf{U}] + \boldsymbol{\epsilon}, \tag{2.2}$$

where $\mathbf{d}$ is the M-dimensional vector of all data collected throughout the smoothing or assimilation period and $\boldsymbol{\epsilon}$ is the measurement error. The operator $\mathcal{L}$ is a vector of linear measurement functionals $\mathcal{L}_m$, $1 \le m \le M$, each of which acts on the entire 10-dimensional vector field $\mathbf{U} = \mathbf{U}(\mathbf{x}, t)$ to produce a single real number. We used monthly mean TAO data for SST (or our model variable T), surface winds ($\mathbf{u}^a$), and the depth of the 20°C isotherm [our $\theta^{(1)} + \theta^{(2)}$]. These data are available via the Internet from the National Oceanic and Atmospheric Association (NOAA) Pacific Marine Environmental Laboratory (PMEL). See Soreide et al. (1996). There are about 2400 scalar data values in our 12-month-long years 1 and 2, and about 4000 values in our 18-month-long year 3. The weighted least squares criterion of best fit to the model and data is the penalty functional $\mathcal{J} = \mathcal{J}[\mathbf{U}, \mathbf{d}]$ defined in section 4 of B98. Briefly, we minimize the weighted squares of the initial error, dynamical error, and observational error summed over space and time as appropriate. The data error covariance is assumed to be diagonal with different error variances for the three data types: SST (0.09 K^2), Z20 (9 m^2), and u^a, v^a (0.25 $\text{m}^2\ \text{s}^{-2}$).

The variance scales and decorrelation scales for the dynamical errors were specified with great difficulty, given our intermediate model. Its vertical resolution is minimal in the extreme and it is an anomaly model that is partially linearized about an estimate of the climatological annual cycle. The parameterizations of unresolved processes are extremely simple. We arbitrarily restricted our considerations of dynamical errors to the unique feature of intermediate models: neglected but numerically resolvable processes such as anomalous momentum advection, volume flux associated anomalous currents and thicknesses, and eddy fluxes of heat owing to tropical instability waves. Our estimates of these residual candidates were based on the amplitudes, spatial scales, and temporal scales of the El Niño anomalies themselves (see Table 1). The amplitudes deduced for the residuals in the 10 prognostic equations are given in Table 2. The notation in the table is that, for example, $\mathbf{r}_u^{(1)}$ is the amplitude of the residual for the oceanic upper-layer momentum balance. Each Cartesian component has the same amplitude. For example, the variance scale

TABLE 1a. Standard deviations of anomalous circulation fields.

Atmosphere	$u_a \sim 5$ m s^{-1}, $v_a \sim 2$ m s^{-1}, $\phi \sim 80$ m^2 s^{-2} or $\rho^a\phi \sim 1$ mb
Ocean upper layer	$u^{(1)}, v^{(1)} \sim 0.5$ m s^{-1}, $\theta^{(1)}, \sim 15$ m, $T \sim 2°$
Ocean lower layer	$u^{(2)}, v^{(2)} \sim 0.5$ m s^{-1}, $\theta^{(2)} \sim 50$ m

TABLE 2. Standard deviations of residuals.

1) Atmosphere	$\mathbf{r}_u^a \sim (10^{-5}$ m s^{-2}, 0.4×10^{-5} m s$^{-2})$, $r_\Phi^a \sim 4.5 \times 10^{-3}$ m^2 s^{-3}
2) Ocean upper layer	$\mathbf{r}_u^{(1)} \sim 0.3 \times 10^{-6}$ m s^{-2}, $r_\theta^{(1)} \sim 7.5 \times 10^{-6}$ m s^{-1} $r_T \sim 2.5 \times 10^{-7}$ K s^{-1}
3) Ocean lower layer	$\mathbf{r}_u^{(2)} \sim 0.5 \times 10^{-6}$ m s^{-2}, $r_\theta^{(2)} \sim 8 \times 10^{-6}$ m s^{-1}

for the residual in the zonal momentum balance in the oceanic upper layer is $(0.3 \times 10^{-6}$ m s$^{-2})^2$. We assume that the amplitudes and scales of the initial residuals are those of the anomalies themselves, that is, we assume that the error in our initial estimate $\mathbf{U}_I$ for the anomalous circulation $\mathbf{U}$ is of the order of 100%. The functional forms of the initial and dynamical error covariances are given in B98, Eqs. (5.1)–(5.3). The forms are stationary in time and zonally homogeneous, but are meridionally inhomogeneous. The forms are maximally simple (Gaussians, Markovians, etc.), and expedite the computation of convolutions.

The total number of computational degress of freedom in the inversions is approximately 4×10^7. This is the number of unknown residuals on the three-dimensional space–time grid. We compute the nonlinear inverse as the limit of a sequence of linear inverses. For each of these there is a null space. The dimension of its complement (i.e., the number of observable degrees of freedom) equals M, the number of data, which is about 3×10^3 (years 1 and 2) or 4×10^3 (year 3). The advantage of the representer algorithm used here is that it restricts the search for each linear inverse to the M-dimensional ''data subspace'' in which the inverse lies (see, e.g., Bennett 1992, section 5.5).

3. Three inversions

a. Year 1: April 1994–March 1995

This inversion was described in full in B98. The principal SST anomaly was a warm pool just east of the data line, reaching a maximum amplitude of about +2.5 K in November 1994 and fading entirely by March 1995. The inverse estimates of SST, Z20, and $\mathbf{u}^a$ fit the observations to within one standard error throughout the year, but the fits to the dynamics significantly exceed standard errors. Time series of anomalies, and contour plots of anomalies and dynamical residuals may be seen in B98. Significance tests will be reported again here in section 4.

b. Year 2: April 1995–March 1996

The period was characterized by a mild La Niña episode with cooler than normal temperatures in December 1995 on the equator reaching from South America to 160°W. The coolest anomalous temperature was about −1.25 K. Our data for year 2 consist of 700 values of anomalous monthly mean SST, 688 values of anomalous monthly mean Z20, and a total of 1256 scalar values of the anomalous surface wind components u^a, v^a. Thus, $M = 700 + 688 + 1256 = 2644$ data values. Every parameter in the model and prior covariances is the same as the values for year 1 that were reported in detail in B98 and are listed in part in Tables 1 and 2 here. The assumed SST error of 0.3 K does not reflect instrumental error, which is closer to 0.1 K. Rather, it is the difference between the upper-layer average temperature T and the temperature recorded by a single shallow thermometer.

The state estimate $\hat{\mathbf{U}} = \hat{\mathbf{U}}(\mathbf{x}, t)$ is found as a solution of the nonlinear Euler–Lagrange equations for extrema of the penalty functional $\mathcal{J} = \mathcal{J}[\mathbf{U}, \mathbf{d}]$. These equations are solved iteratively. For year 1, the sequence of inversions had converged effectively after seven iterations and the effective limit for $\hat{\mathbf{U}}$ was in satisfactory agreement with the data. For year 2, the sequence of inversions had developed small (10%) oscillations after 12 iterates. Each was in fairly satisfactory agreement with the data, so the 12th iterate was taken as an approximate best fit to the dynamics and data. The time series of $\hat{\mathbf{U}}$ at 95°W shown in Fig. 1 include SST, Z20, u^a, and v^a at three TAO moorings: 5°S, 0°, 5°N. Also shown are the monthly mean (30-day averaged) TAO data, and prior estimates of standard errors in the data. Each datum within a panel has the same error bar, but note that the scale varies from panel to panel. The situation on the equator is exceptional; in July and August 1995, the inverse estimates of SST and Z20 fail to fit the TAO data to within or close to within standard errors. The situation extends to 125°W (not shown) and appears to be associated with an extremely narrow equatorial

TABLE 1b. Length and timescales of anomalous circulation fields

	Zonal (m)	Meridional (m)	Time (s)
Atmosphere ($\mathbf{u}^a$, ϕ^a)	10^6	2.5×10^5	10^7
Ocean upper layer [$\mathbf{u}^{(1)}$, $\theta^{(1)}$]	10^6	2.5×10^5	10^7
(T)	3×10^6	10^6	10^7
Ocean lower layer [$\mathbf{u}^{(2)}$, $\theta^{(2)}$] (Roughly: 10^5 m ~ 1°; 10^5 s ≅ 1 day)	3×10^6	5×10^5	10^7

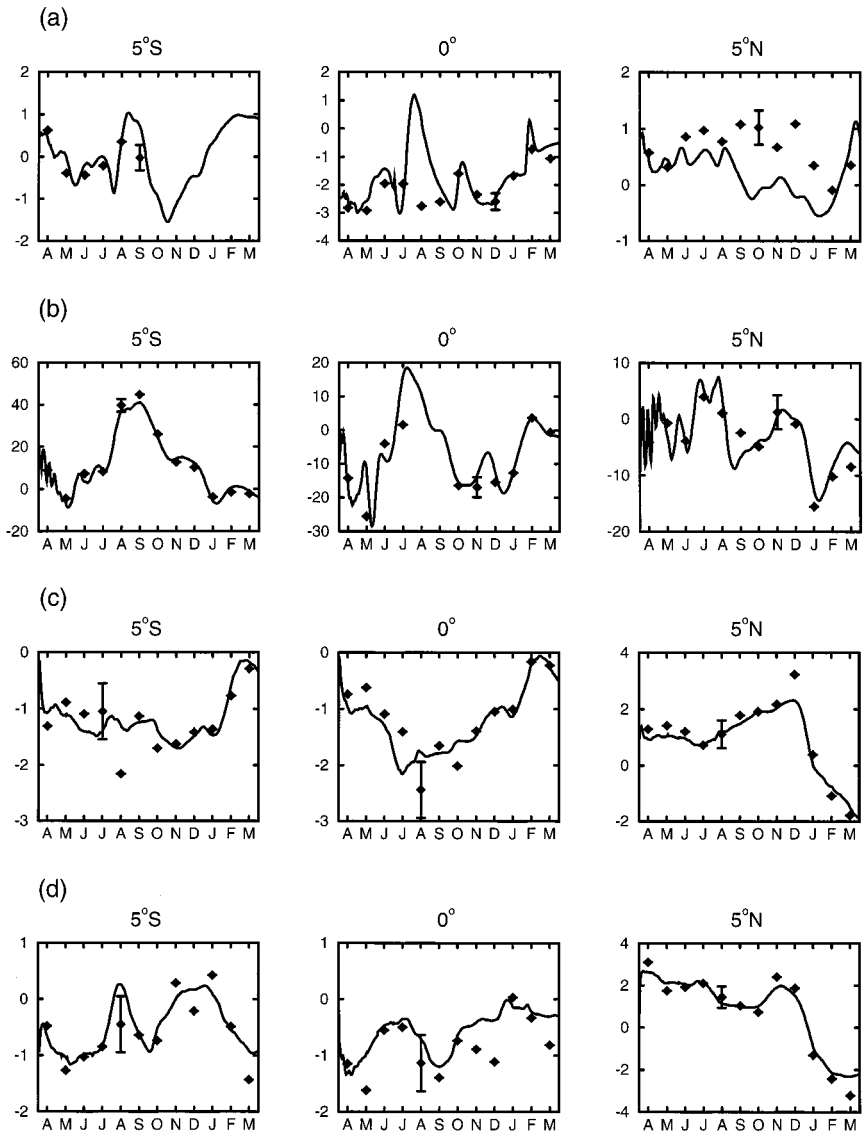

FIG. 1. Time series of $\hat{\mathbf{U}}$, the inverse estimate of the anomalous state at three TAO moorings (5°S, 0°, 5°N) along 95°W. The centered symbols are the 30-day average TAO data. All data of the same type are assigned the same standard error so only one bar is shown per panel, but note that the amplitude scale and bar length vary from panel to panel. Results here are for year 2 (Apr 1995–Mar 1996). (a) SST, ±0.3 K, (b) Z20, ±3 m, (c) u^a, ±0.5 m s^{-1}, and (d) v^a, ±0.5 m s^{-1}.

anomaly extending from the eastern boundary to 140°W (see Fig. 2). The anomaly appears to originate in an eastern boundary feature that in turn is responsible for the oscillation in the sequence of linear inversions.

The residual r_T for the heat equation is shown in Fig. 3a for day 150 (mid-September 1995). Extremely large-amplitude negative residuals (−3 standard errors) exist on the equator at 95°W. This was the peak; the duration of the residuals was about 100 days, which is the time-scale imposed in the prior error variance for the dynamics. Their meridional extent of ±1000 km was also imposed through their prior covariance. The role of the residual is to correct the wildly swinging inverse SST toward the TAO data. Clearly the model has a mode of error that is of much narrower extent than assumed, and so the inverse is unable to correct for this mode when such errors are present.

The residuals $\mathbf{r}_u^{(i)}$ for the oceanic momentum equations in layers 1 and 2 are not significantly large, save for the meridional momentum equation in layer 2 (see Fig. 3b). The equatorial residual exceeds three standard errors at day 150 from the east boundary to 140°W. The residual in effect ''drives'' the meridionally antisymmetric part of the lower-layer thickness. See Fig. 1b, especially 5°N and 5°S where Z20 is actually identified with $\theta^{(1)} + \theta^{(2)}$. Note the opposing tendencies in Sep-

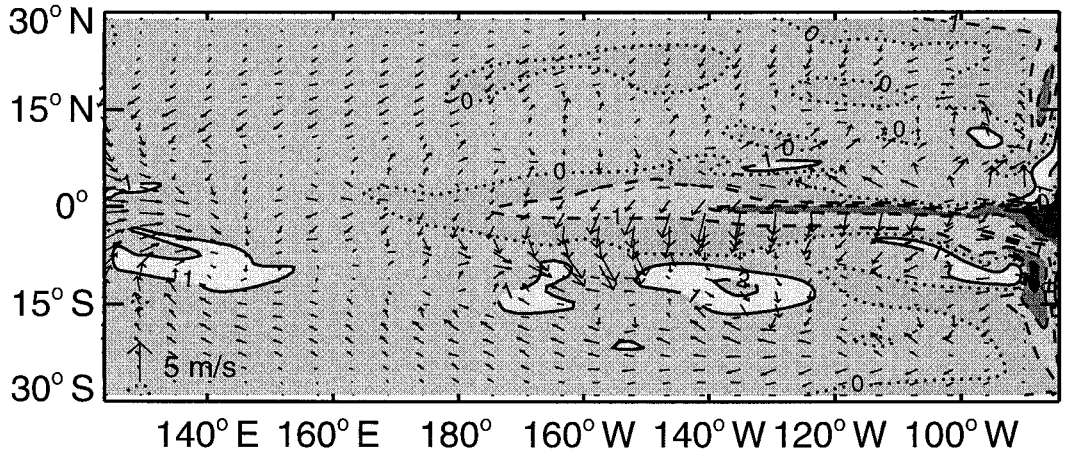

FIG. 2. Inverse estimates of anomalous SST and winds, year 2 day 180 (mid-Nov, 1995). The contour interval for SST is 1 K; the wind speed scale is shown lower left.

tember. The inverse estimates of the residuals are linear combinations of the model error covariances [Bennett 1992, Eq. (5.4.19)]. The last mentioned are symmetric here, by hypothesis, and evidently the combination that would yield the appropriate antisymmetric residual or ''driving'' $r_\theta^{(2)}$ for the lower-layer thickness equation must incur a greater penalty than the symmetric residual $r_v^{(2)}$ for the lower-layer meridional momentum equation. The residual $r_\theta^{(2)}$ is shown in Fig. 3c for day 150; it is locally significantly large (two standard errors); it is indeed meridionally symmetric but not about the equator. As reported in B98, the inverse uses complicated multivariate residuals in order to track the thickness data with minimal penalty. The residuals in the atmospheric dynamics are not significantly large. This is a consequence of the weakness of the TAO wind anomalies.

c. Year 3: December 1996–May 1998

The period was characterized by a much-studied major El Niño event (e.g., McPhaden 1999a,b). Equatorial temperature anomalies reached +5 K near South America in November 1997, while Z20 anomalies reached −70 m in the western Pacific and +100 m near South America. Our data for year 3 consist of 1088 values of anomalous monthly mean SST, 1058 values of anomalous monthly mean Z20, and a total of 1862 scalar values of the anomalous surface wind components u^a, v^a. Thus $M = 4008$ data values. Every parameter in the model and in the prior covariances is the same as those for years 1 and 2. The sequence of inversions converged after 8 iterations to a well-defined limit. The time series at 95°W shown in Fig. 4 include SST, Z20, u^a, and v^a at the TAO moorings, along with 30-day-averaged TAO data and standard errors in the data. The inverse tracks the large observed anomalies with remarkable skill. Inverse estimates of anomalous SST and winds for mid-December 1997 are shown in Fig. 5a; inverse estimates of anomalous Z20 for the same month are shown in Fig. 5b. The great amplitude of the major El Niño event is again evident. It also differs in character from the milder event of year 1; that earlier event involved a +2-K warming near the dateline rather than a +5-K warming off South America.

The residual r_T for the temperature equation, day 360 (mid-December 1997), is contoured in Fig. 6a. The amplitude exceeds two standard errors from 100° to 140°W on either side of the equator. The SST anomaly was at its peak at that time, so the need for a heat source is not apparent. The residual $r_v^{(2)}$ for the lower-layer meridional momentum equation is shown in Fig. 6b. A minimum value of almost minus five standard errors is attained on day 360 (mid-December 1997), on the equator at 95°W. Again this is evidence of the multivariate nature of the analysis system; $v^{(2)}$ is not observed at all, but meridionally asymmetrical layer thicknesses $\theta^{(2)}$ are present in the TAO data. The residual $r_\theta^{(2)}$ for lower-layer thickness on day 180 (mid-May 1997) is shown in Fig. 6c. The maximum exceeds two plus standard errors on the equator at 155°W, the minimum is as low as minus two standard errors on the equator at 95°W. The thickness is nonetheless increasing at 95°W in May 1997 (see Fig. 4b), but evidently too fast in the unforced or residual-free model dynamics and so a negative residual obtains.

Atmospheric momentum residuals $\mathbf{r}_u^a$ barely exceed standard errors save at day 360 (mid-December 1997), near 120°W (not shown). This is surprising as the atmospheric model is very crude, yet the wind data are fit well (see Figs. 4c,d).

4. Significance tests

The penalty functional $\mathcal{J}$ is quadratic in the initial, dynamical, and observational residuals. It is not quadratic in the state **U**, because the dynamical operator is nonlinear. There is anomalous advection of heat anomaly in the ocean and the wind stress law is quadratic in

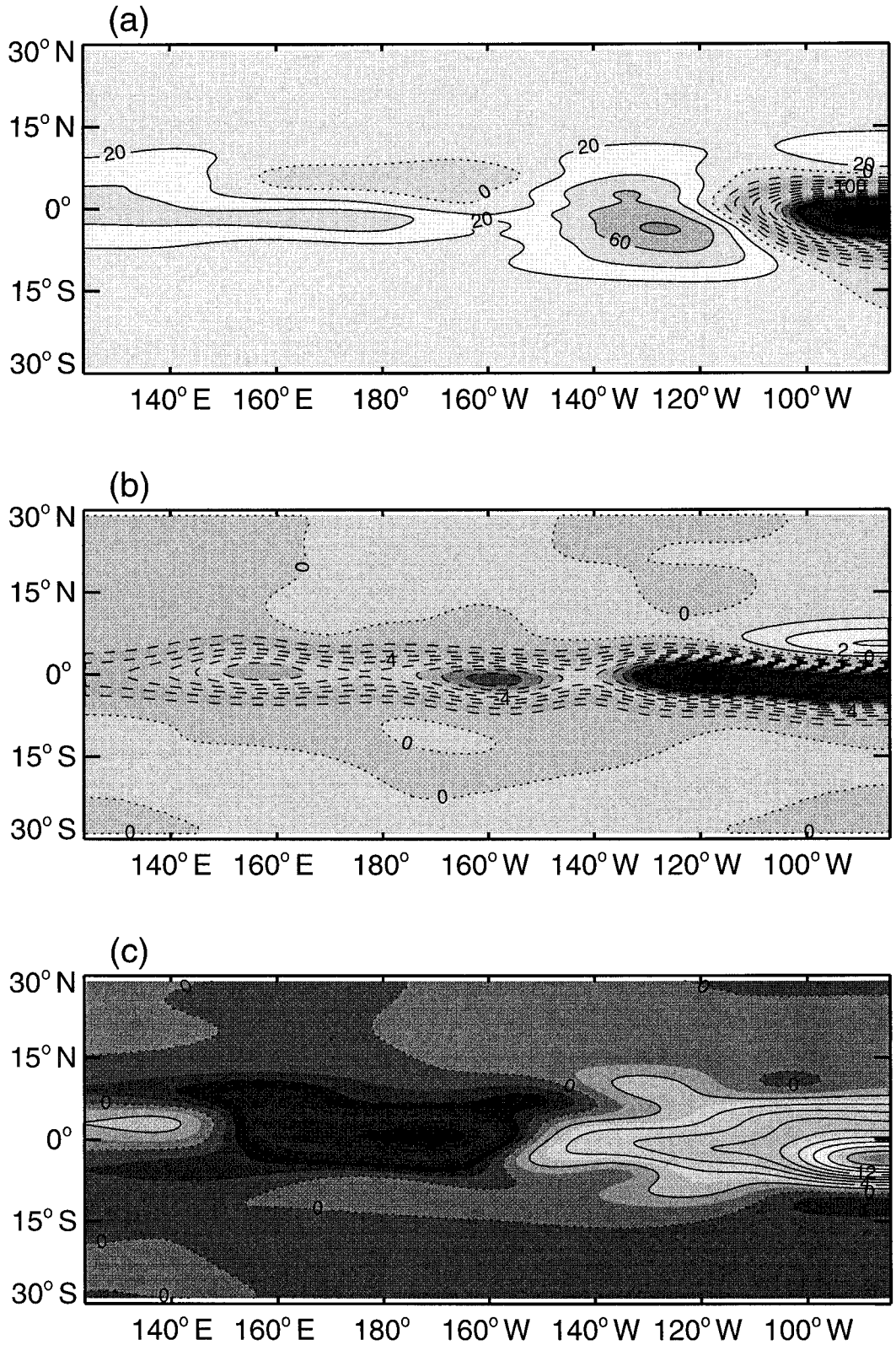

FIG. 3. Residuals for (a) heat equation on year 2 day 150 (mid-Sep 1995), contour interval 20 W m^{-2}; (b) oceanic lower-layer meridional momentum equation on day 150, contour interval 10^{-7} m s^{-2}; (c) oceanic lower-layer thickness equation on day 150, contour interval 2×10^{-6} m s^{-1}.

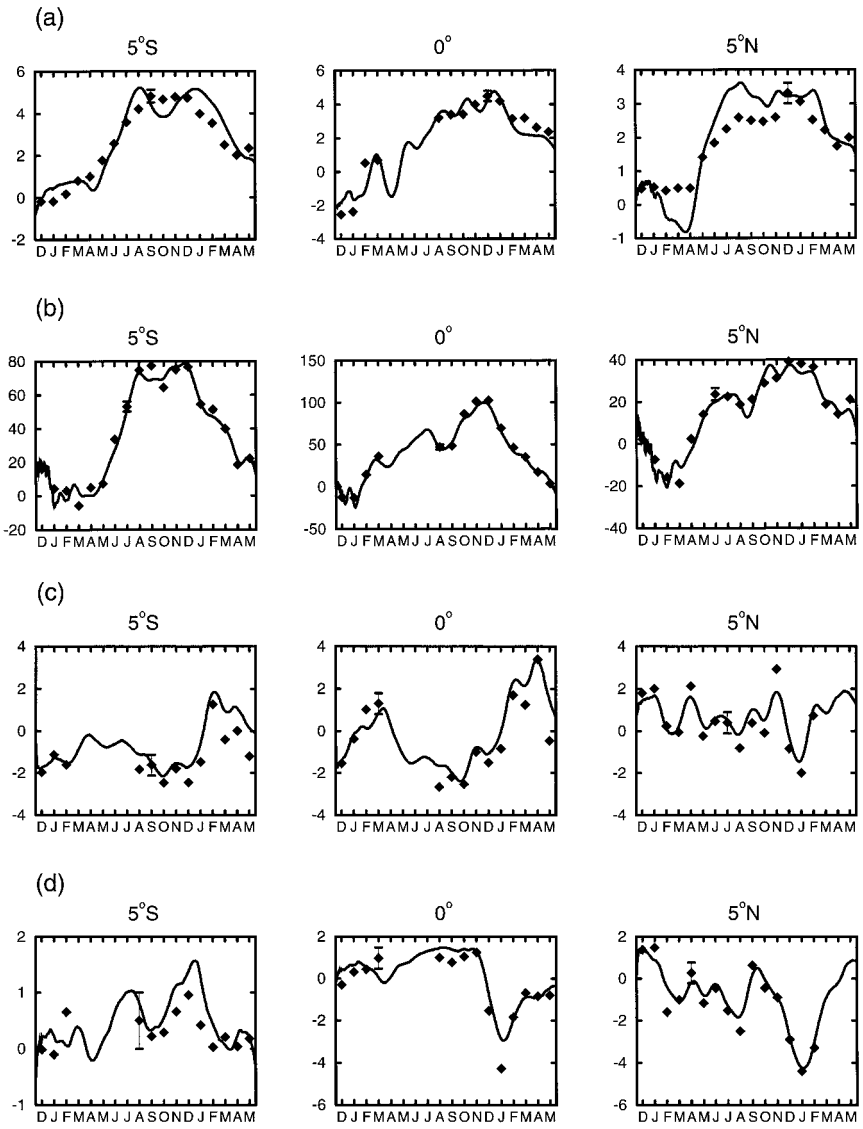

FIG. 4. As in Fig. 1, for year 3 (Dec 1996–May 1998).

the wind anomalies. However we minimize $\mathcal{J}$ with respect to $\mathbf{U}$ via a sequence of linear minimization problems. In each problem the nonlinear dynamical operator is replaced by a linearization about the minimizer of the previous problem (Bennett 1992, section 7.5). Then $\mathcal{J}$ becomes the test statistic for $\mathcal{H}_0$, our set of hypothetical prior error covariances [see also B98, (4.12)–(4.13)]. More precisely, if $\mathcal{H}_0$ is true then the minimum value $\hat{\mathcal{J}} \equiv \mathcal{J}[\hat{\mathbf{U}}, \mathbf{d}]$ is χ^2_M, the chi-squared random variable with M degrees of freedom where M is the total number of data. The first moments of $\hat{\mathcal{J}}$ are therefore

$$E\chi^2_M = M,$$
$$\mathrm{var}\chi^2_M \equiv E(\chi^2_M)^2 - (E\chi^2_M)^2 = 2M. \qquad (4.1)$$

The mean value M is about 2600 for years 1 and 2 and about 4000 for year 3. The standard deviation $\sigma \equiv \sqrt{2M}$ is thus about 70 for years 1 and 2 and 90 for year 3.

Let $\mathbf{h}$ denote the difference between the data and measured values of the forward solution $\mathbf{U}_F$ (i.e., measured values of the model solution with initial value $\mathbf{U}_I$):

$$\mathbf{h} \equiv \mathbf{d} - \mathcal{L}[\mathbf{U}_F]. \qquad (4.2)$$

It may be shown (Bennett 1992, section 5.5) that the reduced value of the penalty functional $\mathcal{J}$ is

$$\hat{\mathcal{J}} \equiv \mathcal{J}[\hat{\mathbf{U}}, \mathbf{d}] = \mathbf{h}^{\mathrm{T}}\mathbf{P}^{-1}\mathbf{h}, \qquad (4.3)$$

where $\mathbf{P} = \mathbf{R} + \mathbf{C}_{\epsilon\epsilon}$, $\mathbf{R}$ being the $M \times M$ symmetric positive-definite representer matrix (Bennett 1992, section 5.5) and $\mathbf{C}_{\epsilon\epsilon}$ the prior error covariance matrix for the data. The matrix $\mathbf{R}$ is equivalent to the covariance of measured values of random solutions of the forward

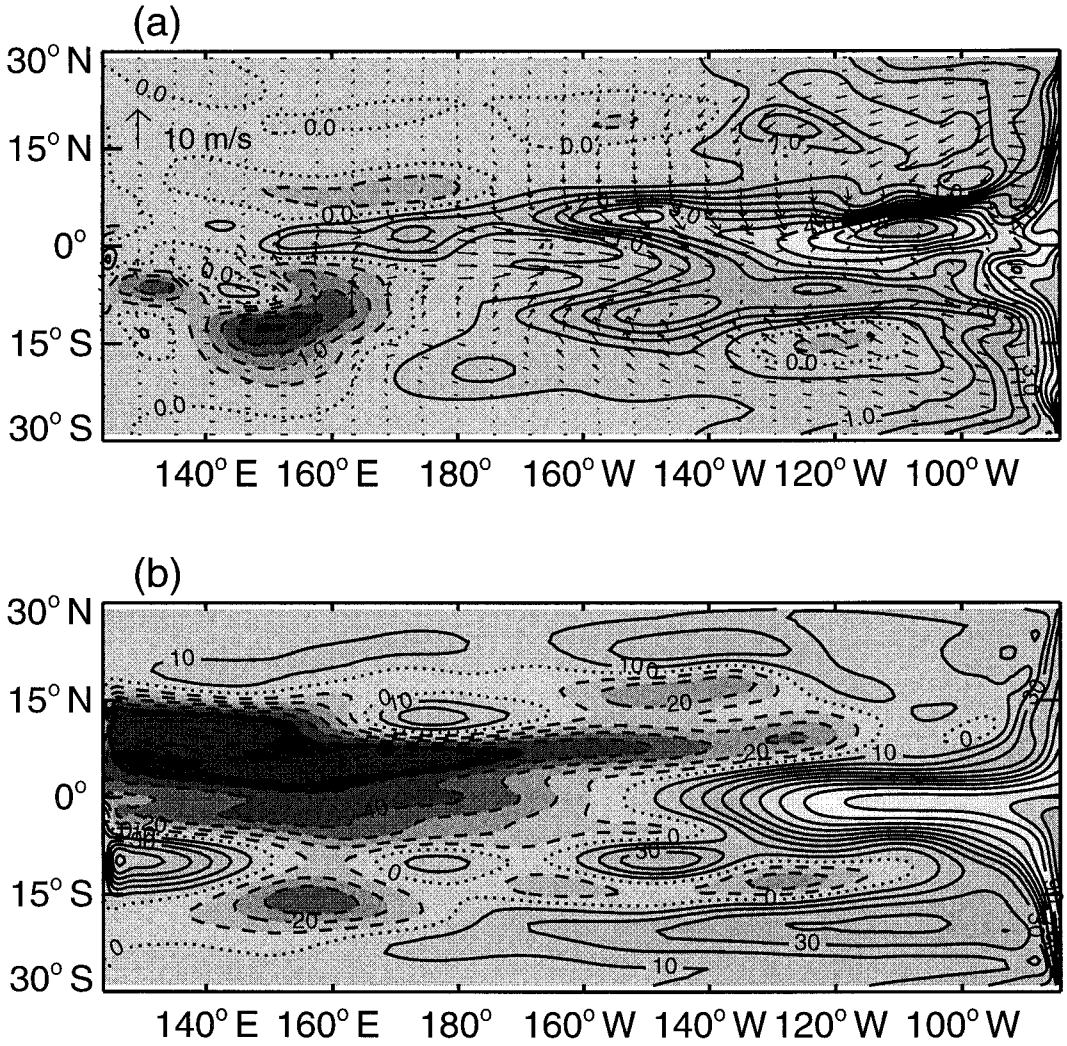

FIG. 5. (a) Anomalous SST and winds for year 3 day 360 (mid-Dec 1997), contour interval 0.5 K; (b) anomalous Z20 (mid-Dec 1997), contour interval 10 m.

linearized model, in response to random forcing and random initial conditions having the same first and second moments as we hypothesize for our dynamical and initial errors. It may also be shown that

$$E\mathbf{h} = 0, \qquad E\mathbf{h}\mathbf{h}^{\mathrm{T}} = \mathbf{P} \tag{4.4}$$

(Bennett 1992, section 5.6). Defining a scaled prior data misfit by $\mathbf{h}' = \mathbf{P}^{-1/2}\mathbf{h}$, it is evident from (4.4) that $E\mathbf{h}'\mathbf{h}'^{\mathrm{T}} = \mathbf{I}$, where $\mathbf{I}$ is the $M \times M$ unit matrix so $\hat{\jmath} = \mathbf{h}'^{\mathrm{T}}\mathbf{h} = \chi^2_M$. Strictly speaking, each component of $\mathbf{h}'$ should be Gaussian, but we note that each component is a linear combination of those of $\mathbf{h}$ and we invoke the central limit theorem.

Other values of the penalty functional are available. The prior value is

$$\jmath_F \equiv \jmath[\mathbf{U}_F, \mathbf{d}] = \mathbf{h}^{\mathrm{T}}\mathbf{C}_{\epsilon\epsilon}^{-1}\mathbf{h}. \tag{4.5}$$

Hence using (4.4) the expected value is

$$E\jmath_F = E\ \mathrm{Tr}(\mathbf{C}_{\epsilon\epsilon}^{-1/2}\mathbf{h}\mathbf{h}^{\mathrm{T}}\mathbf{C}_{\epsilon\epsilon}^{-1/2}) = \mathrm{Tr}(\mathbf{C}_{\epsilon\epsilon}^{-1/2}\mathbf{P}\mathbf{C}_{\epsilon\epsilon}^{-1/2}), \tag{4.6}$$

where Tr is the matrix trace. It may be shown (Bennett 1992, section 5.6) that

$$\mathcal{L}[\hat{\mathbf{U}}] = \mathcal{L}[\mathbf{U}_F] + \mathbf{R}\mathbf{P}^{-1}\mathbf{h}, \tag{4.7}$$

so the misfit of the inverse to the data is

$$\mathbf{d} - \mathcal{L}[\hat{\mathbf{U}}] = \mathbf{C}_{\epsilon\epsilon}\mathbf{P}^{-1}\mathbf{h}. \tag{4.8}$$

Hence the reduced data penalty is

$$\begin{aligned}\hat{\jmath}_{\mathrm{data}} &\equiv (\mathbf{d} - \mathcal{L}[\hat{\mathbf{U}}])^{\mathrm{T}}\mathbf{C}_{\epsilon\epsilon}^{-1}(\mathbf{d} - \mathcal{L}[\hat{\mathbf{U}}]) \\ &= \mathbf{h}^{\mathrm{T}}\mathbf{P}^{-1}\mathbf{C}_{\epsilon\epsilon}\mathbf{P}^{-1}\mathbf{h}\end{aligned} \tag{4.9}$$

with expected value

$$\begin{aligned}E\hat{\jmath}_{\mathrm{data}} &= E\ \mathrm{Tr}(\mathbf{C}_{\epsilon\epsilon}^{1/2}\mathbf{P}^{-1}\mathbf{h}\mathbf{h}^{\mathrm{T}}\mathbf{P}^{-1}\mathbf{C}^{1/2}) \\ &= \mathrm{Tr}(\mathbf{C}_{\epsilon\epsilon}^{1/2}\mathbf{P}^{-1}\mathbf{C}_{\epsilon\epsilon}^{1/2}).\end{aligned} \tag{4.10}$$

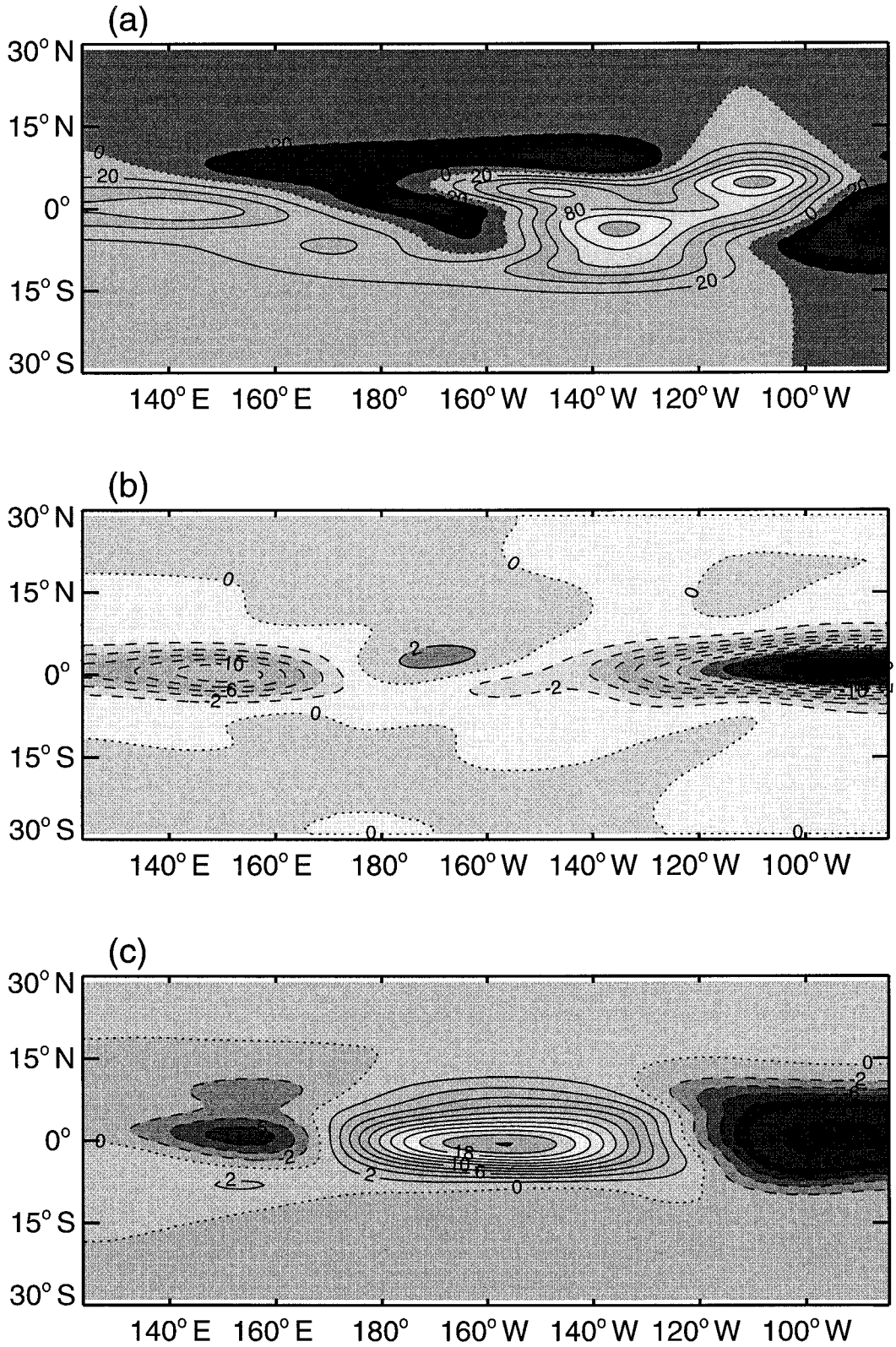

FIG. 6. Residuals for (a) heat equation on year 3 day 360 (mid-Dec 1997), contour interval 20 W m^{-2}; (b) oceanic lower-layer meridional momentum equation on year 3 day 360 (mid-Dec 1997), contour interval 2×10^{-7} m s^{-2}; (c) oceanic lower-layer thickness equation on year 3 day 180 (mid-May 1997), contour interval 2×10^{-6} m s^{-1}.

TABLE 3a. Expected and actual values.

	Year 1 $M = 2624$, $\sqrt{2M} = 72$		Year 2 $M = 2644$, $\sqrt{2M} = 73$		Year 3 $M = 4008$, $\sqrt{2M} = 89$	
	Expected	Actual	Expected	Actual	Expected	Actual
$\mathcal{J}_F$	160 000	35 708	156 000	32 028	246 132	132 140
$\hat{\mathcal{J}}_{\text{mod}}$	1015	1614	1022	1650	1458	3680
$\hat{\mathcal{J}}_{\text{SST}}$	(689)	419	(700)	717	(1088)	995
$\hat{\mathcal{J}}_{u^a}$	(624)	453	(628)	383	(931)	1546
$\hat{\mathcal{J}}_{v^a}$	(624)	396	(628)	380	(931)	940
$\hat{\mathcal{J}}_{Z20}$	(687)	820	(680)	678	(1058)	1129
$\hat{\mathcal{J}}_{\text{data}}$	1609	2088	1622	2160	2550	4614
$\hat{\mathcal{J}}$	2624	3702	2644	3810	4008	8322

Subtracting (4.3) and (4.9) yields the reduced model penalty

$$\hat{\mathcal{J}}_{\text{mod}} = \mathbf{h}^{\text{T}}\mathbf{P}^{-1}\mathbf{R}\mathbf{P}^{-1}\mathbf{h} \tag{4.11}$$

with expected value

$$E\hat{\mathcal{J}}_{\text{mod}} = \text{Tr}(\mathbf{R}^{1/2}\mathbf{P}^{-1}\mathbf{R}^{1/2}). \tag{4.12}$$

Note that $\hat{\mathcal{J}}_{\text{mod}}$ includes penalties for both the dynamical residual and the initial residual. These penalties can be separated using the Euler–Lagrange equations, but the computations are awkward and were not attempted here. Formulas for the variances of $\mathcal{J}_F$, $\hat{\mathcal{J}}_{\text{data}}$, and $\hat{\mathcal{J}}_{\text{mod}}$ may be derived as follows. To begin, rotate and scale the first-guess data misfit:

$$\mathbf{h}' = \mathbf{P}^{-1/2}\mathbf{h}, \qquad E\mathbf{h}' = 0, \qquad E\mathbf{h}'\mathbf{h}'^{\text{T}} = \mathbf{I}. \tag{4.13}$$

Then the first-guess penalty is

$$\mathcal{J}_F = \mathbf{h}'\mathbf{Q}\mathbf{h}', \tag{4.14}$$

where $\mathbf{Q} = \mathbf{P}^{1/2}\mathbf{C}_{\epsilon\epsilon}^{-1}\mathbf{P}^{1/2}$ is symmetric positive-definite and may be diagonalized:

$$\mathbf{Q} = \mathbf{U}\mathbf{\Lambda}\mathbf{U}^{\text{T}}, \qquad \mathbf{U}\mathbf{U}^{\text{T}} = \mathbf{U}^{\text{T}}\mathbf{U} = \mathbf{I}, \tag{4.15}$$

and $\mathbf{\Lambda} = \text{diag}(\lambda_1, \ldots, \lambda_M)$ is diagonal. A further rotation yields

$$\mathcal{J}_F = \mathbf{j}^{\text{T}}\mathbf{\Lambda}\mathbf{j} = \sum_{m=1}^{M} \lambda_m j_m^2, \tag{4.16}$$

where

$$\mathbf{j} = \mathbf{U}^{\text{T}}\mathbf{h}', \qquad E\mathbf{j} = 0, \qquad E\mathbf{j}\mathbf{j}^{\text{T}} = \mathbf{I}. \tag{4.17}$$

As before, the mean prior penalty is

$$E\mathcal{J}_F = \sum_{m=1}^{M} \lambda_m = \text{Tr}(\mathbf{Q}) = \text{Tr}(\mathbf{P}^{1/2}\mathbf{C}_{\epsilon\epsilon}^{-1}\mathbf{P}^{1/2}). \tag{4.18}$$

TABLE 3b. Standard deviations.

	Year 1	Year 2	Year 3
$\mathcal{J}_F$	136 000	131 000	146 057
$\hat{\mathcal{J}}_{\text{mod}}$	38	38	72
$\hat{\mathcal{J}}_{\text{data}}$	60	59	45
$\hat{\mathcal{J}}$	72	73	89

Consider the components of $\mathbf{j}$. Each of the j_m is a weighted sum of components of $\mathbf{h}'$, and the weights for j_m, j_n are orthonormal if $n \neq m$ [see (4.15)]. It follows that the j_m are asymptotically normal $N(0, 1)$ random variables [see (4.17)] and that j_m, j_n are uncorrelated and so independent if $n \neq m$. It follows after a little algebra that

$$E\mathcal{J}_F^2 - (E\mathcal{J}_F)^2 = 2\sum_{m=1}^{M} \lambda_m^2, \tag{4.19}$$

that is,

$$\text{var}\mathcal{J}_F = 2\ \text{Tr}(\mathbf{C}_{\epsilon\epsilon}^{-1}\mathbf{P}^2\mathbf{C}_{\epsilon\epsilon}^{-1}). \tag{4.20}$$

The central limit theorem also implies that $\mathcal{J}_F$, like χ_M^2, is asymptotically normal as $M \to \infty$.

It may similarly be shown that as $M \to \infty$,

$$\text{var}\,\hat{\mathcal{J}}_{\text{data}} = 2\ \text{Tr}(\mathbf{C}_{\epsilon\epsilon}\mathbf{P}^{-2}\mathbf{C}_{\epsilon\epsilon}), \tag{4.21}$$

$$\text{var}\,\hat{\mathcal{J}}_{\text{mod}} = 2\ \text{Tr}[(\mathbf{I} - \mathbf{P}^{-1/2}\mathbf{C}_{\epsilon\epsilon}\mathbf{P}^{-1/2})^2], \tag{4.22}$$

and both $\hat{\mathcal{J}}_{\text{data}}$ and $\hat{\mathcal{J}}_{\text{mod}}$ are asymptotically normal.

Values for the various $\mathcal{J}$ are listed in Table 3a. Parenthetical values are numbers of data of a given type; they are not expected values. Only $E\hat{\mathcal{J}} = M$, the total number of data (last row). The standard deviations given in Table 3b are the square roots of variances computed as in (4.20)–(4.22).

The first row of Table 3a indicates that the forward model is much better than expected. Nevertheless the actual values of $\mathcal{J}_F$ are much larger than is desirable. We would *like* each data misfit to be a standard error of measurement or less, that is, we would *like* $\mathcal{J}_F$ to be equal to M or less. Such would be the case if the dynamics and initial conditions were perfect. The last row indicates that the inverse estimate $\hat{\mathcal{J}}$ is much worse than expected. Recall that the standard deviation of $\hat{\mathcal{J}}$ is $\sigma = \sqrt{2M}$, which is given at the top of the table. The actual values of $\hat{\mathcal{J}}$ exceed the expected values by, respectively, 15σ, 16σ, and 49σ in years 1, 2, and 3. The excess is roughly apportioned 45% to $\hat{\mathcal{J}}_{\text{mod}}$ and 55% to $\hat{\mathcal{J}}_{\text{data}}$ in each year.

Given that the three tests cover widely divergent climatological extremes, we are forced to reject our null hypothesis $\mathcal{H}_0$ for the first two moments of the errors

in the model and in the data. Some revisions of $\mathcal{H}_0$ will now be contemplated.

The penalty functional $\mathcal{J}$ is inversely proportional to the prior error covariances for the dynamics, initial condition, and data [see B98, (4.6)–(4.11)]. Hence, increasing all prior covariances by the same factor ψ would lead to *exactly* the same best-fit $\hat{\mathbf{U}}$ for the original nonlinear inverse problem defined by $\mathcal{J}$, since an extremum of $\mathcal{J}$ is also an extremum of $\psi^{-1}\mathcal{J}$. It would of course be more interesting to consider nonuniform rescalings of the priors, but we are focused here on the general issue of ''tuning'' $\mathcal{H}_0$ in light of $\hat{\mathcal{J}}$ being the test statistic, and the uniform rescaling $\mathcal{H}_0 \rightarrow \psi\mathcal{H}_0$ enables a discussion at no computational cost. It follows that if we were to increase all the prior covariances in $\mathcal{H}_0$ by, respectively 40%, 44%, and 108% in years 1, 2, and 3, then the actual value of $\hat{\mathcal{J}}$ would equal its expected value M in each year. These increases correspond to, respectively, 20%, 22%, and 44% increases in standard errors. Now the amplitude scales upon which $\mathcal{H}_0$ is based are certainly not well enough known for such moderate increases to be contested. The data errors are probably just about that well known. The weaker null hypothesis ''$\psi\mathcal{H}_0$'' would not have been rejected by any of the three TAO datasets considered here. Since $\psi\mathcal{H}_0$ is as plausible as $\mathcal{H}_0$, should we conclude that our intermediate model is in fact, validated by the three datasets? Reviewing the sequence of the exercise more carefully, we must conclude that year 1 would have rejected $\mathcal{H}_0$ in favor of $\psi\mathcal{H}_0$ (where $\psi = 1.40$), year 2 would not have rejected $\psi\mathcal{H}_0$ (where $\psi = 1.40$). Year 3 would have rejected $\psi\mathcal{H}_0$ (where $\psi = 1.40$ or 1.44) in favor of the last hypothesis $\psi\mathcal{H}_0$ (where $\psi = 2.08$) that remains untested on an independent dataset.

5. Term balances

The model may be tested more discriminatingly by examining a posteriori term balances. It will be seen that it suffices to consider the balances arising from the inversions as actually carried out with the original null hypothesis $\mathcal{H}_0$, rather than inversions with the even weaker hypotheses $\psi\mathcal{H}_0$. We shall now present term balances for the heat equation:

$$\underbrace{\frac{\partial T}{\partial t}}_{1} + \underbrace{\mathbf{u}^{(1)} \cdot \boldsymbol{\nabla}(\overline{T} + T)}_{2} + \underbrace{\overline{\mathbf{u}}^{(1)} \cdot \boldsymbol{\nabla} T}_{3} + \underbrace{(\mathcal{M} - \overline{\mathcal{M}})\frac{\partial \overline{T}}{\partial z}}_{4} + \underbrace{\mathcal{M}\frac{\partial T}{\partial z}}_{5} + \underbrace{\alpha_S T}_{6} = r_T, \quad (5.1)$$

and for the lower-layer thickness equation:

$$\underbrace{\frac{\partial \theta^{(2)}}{\partial t}}_{1} + \underbrace{H^{(2)}\boldsymbol{\nabla} \cdot \mathbf{u}^{(2)}}_{2} + \underbrace{\epsilon\theta^{(2)}}_{3} = r_\theta^{(2)}. \quad (5.2)$$

The symbols T, θ, and $\mathbf{u}$ denote anomalies of temperature, layer thickness, and velocity, respectively. Overbars indicate annual cycles. Superscripts indicate the layer. The mixing function $\mathcal{M}$ is the Heaviside function of vertical velocity, where the latter is defined by its value $H^{(1)}\boldsymbol{\nabla} \cdot \mathbf{u}^{(1)}$ at the base of the mixed layer (see B98 for further details).

Shown in Fig. 7 are partial term balances for the heat equation for year 1 day 180. Figure 7a shows, in units of watts per meter squared, the local rate of change plus the horizontal advection by anomalous currents (1 + 2). The zonal advection is comparable to the local rate of change; the meridional advection is smaller by factors of 4 and more. The individual contributions 1 and 2 to 7a have much smaller meridional scales than does their sum 1 + 2. Figure 7b, which is the sum 1 + 2 + 3, shows the impact of horizontal advection by the annual cycle. The vertical mixing terms 4, 5 are significant only between 115° and 110°W, 0° to 8°S. Term 4 is positive, 5 is negative and of comparable amplitude wherever both are significant. Term 6 is negligible. Figure 7c is the residual $r_T = (1 + 2 + 3 + 4 + 5 + 6)$.

Shown in Fig. 8 are partial term balances for the lower-layer thickness equation for year 1, day 180. Figure 8a shows, in units of 10^{-6} m s^{-1}, the local rate of change (1). The maximum is 1.6×10^{-5} m s^{-1} on the equator at 145°W. Figure 8b is the total divergence (2). The meridional and zonal components (not shown) are in magnitude twice as large as the total. Figure 8c is the residual $r_\theta^{(2)} = (1 + 2 + 3)$. It is evident, from the major imbalances in these two equations alone that the inverse estimate is not even approximately consistent with the model in year 1. The situation is the same in year 2 (not shown).

Time series of term balances for T and $\theta^{(2)}$ in year 3 are shown in Fig. 9. The location for Fig. 9a is (3.5°S, 135.85°W), where the residual r_T has a local maximum in space on day 360 (mid-December 1997). The time series are actually time sequences of values on days, spaced 30 days apart, and joined by straight line segments for clarity. Not every term in (5.1) is shown; just local acceleration T_t, advection by anomalous zonal velocity $u^{(1)}(\overline{T} + T)_x$, advection by climatological zonal velocity $\overline{u}^{(1)}T_x$, anomalous vertical mixing $\mathcal{M}T_z$, and the residual r_T. The last mentioned is the dominant term, that is, there is no closure in the upper-layer heat budget. The location for Fig. 9b is (0.5°S, 156.38°W), where the residual $r_\theta^{(2)}$ has a local maximum in space on day 180 (mid-June 1997). Values are again daily, spaced 30 days apart. All terms in (5.2) are shown; the individual components $H^{(2)}u_x^{(2)}$ and $H^{(2)}v_y^{(2)}$ are twice as large in magnitude as is their sum $H^{(2)}\boldsymbol{\nabla} \cdot \mathbf{u}^{(2)}$. Even so, the residual $r_\theta^{(2)}$ is about as large in magnitude as either the total divergence or the local rate of change $\theta_t^{(2)}$. There is no closure in the lower-layer mass budget. We must concede that these outcomes could have been anticipated from simple estimates based on the anomaly scales in Table 1 and residual scales in Table 2. The fact that

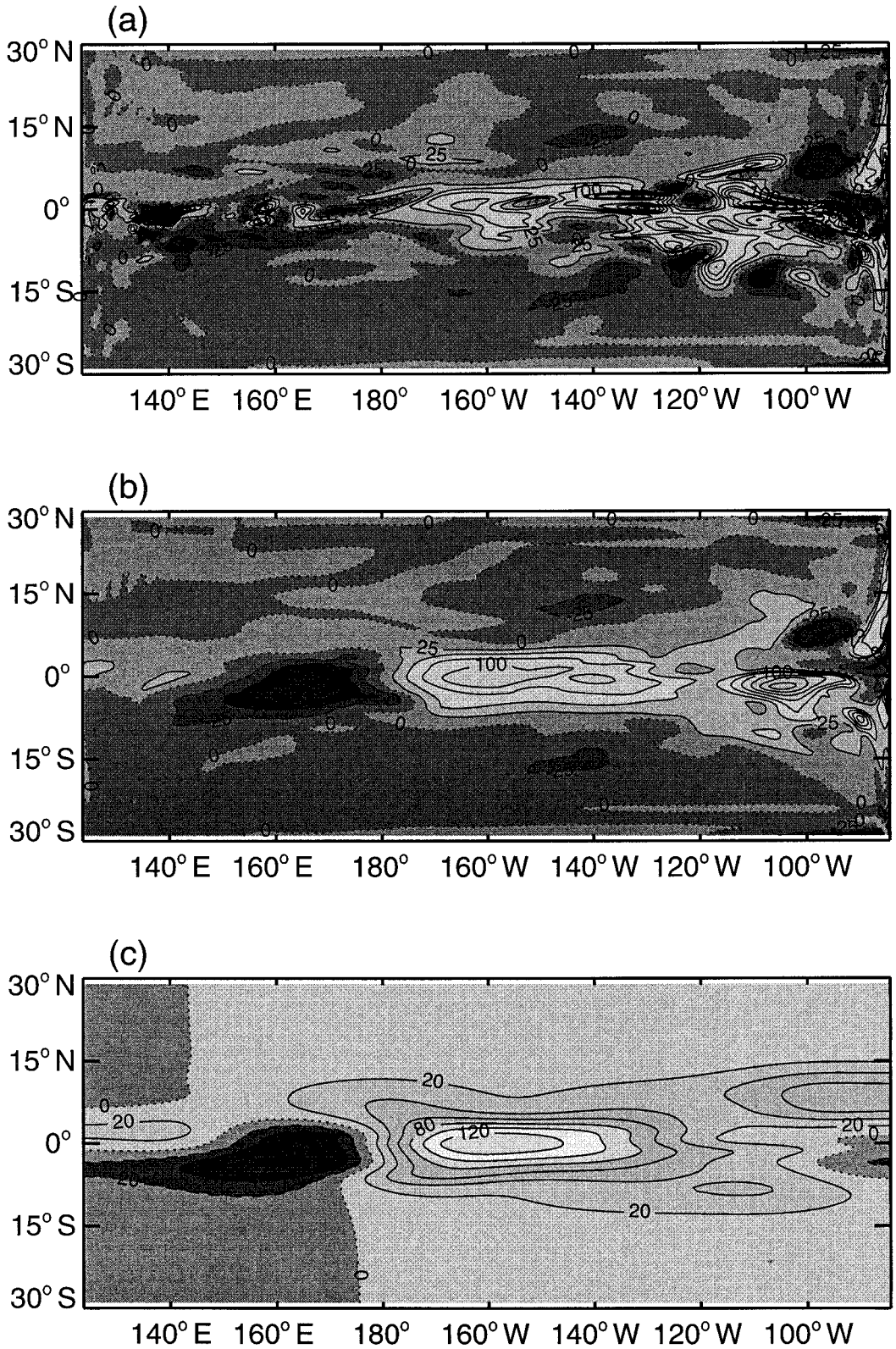

FIG. 7. (a) Terms 1 + 2 of the heat equation (5.1) for year 1 day 180 (mid-Oct 1994), contour interval 25 W m^{-2}; (b) terms 1 + 2 + 3, contour interval 25 W m^{-2}; (c) all terms 1 + 2 + 3 + 4 + 5 + 6 = residual r_T, contour interval 20 W m^{-2}.

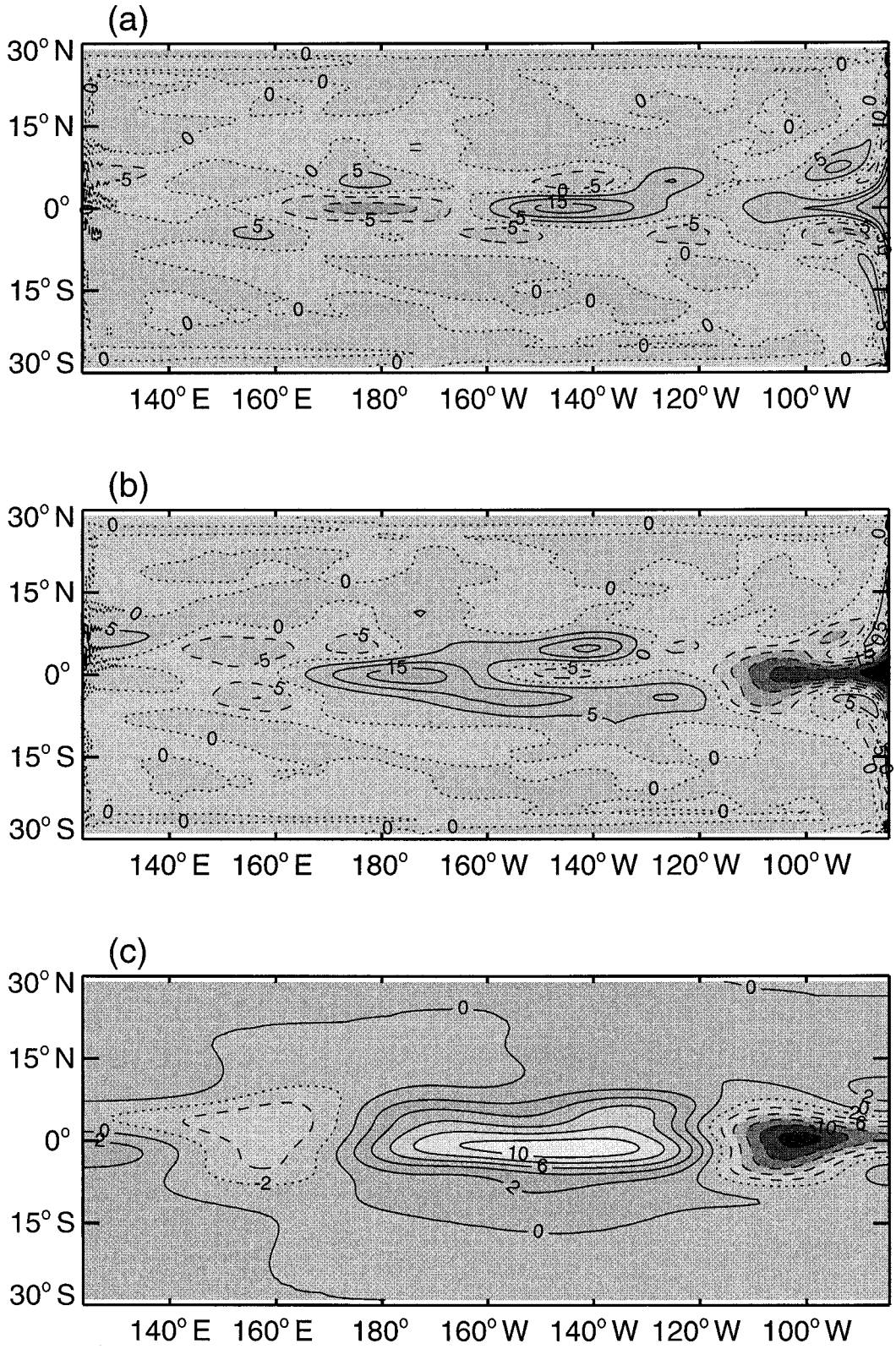

FIG. 8. (a) Term 1 only of the oceanic lower-layer thickness equation (5.2) for year 1 day 180, contour interval = 5×10^{-5} m s^{-1}; (b) term 2 only, contour interval = 5×10^{-5} m s^{-1}; (c) terms 1 + 2 + 3 = residual $r_\theta^{(2)}$, contour interval = 2×10^{-6} m s^{-1}.

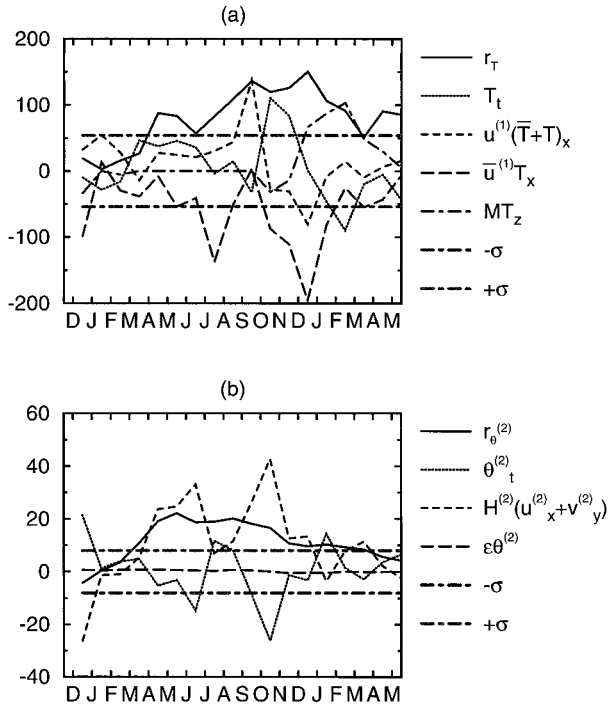

FIG. 9. (a) Time series of year 3 term balances for (a) Eq. (5.1) (W m^{-2}) at (3.5°S, 135.85°W) and (b) Eq. (5.2) in 10^{-6} m s^{-1} at (0.5°S, 156.38°W). All are daily values, spaced 30 days apart and joined by line segments for clarity. The standard error σ in (a) is 54 W m^{-2}, in (b) it is 8×10^{-6} m s^{-1}.

the forward model was *unexpectedly good* for all 3 yr (see Table 3) would suggest that the residual scales were excessively pessimistic. Actual inversions were required in order to learn that the residual scales were in fact optimistic. This seeming paradox is resolved by an analysis of the conditioning of the inversions, or more specifically the conditioning of **P**, the stabilization of the representer matrix (see the appendix). The paradox is entirely feasible. It arises whenever the prior or forward model misfit **h** has unexpectedly large projections on the eigenvectors of **P** having smaller eigenvalues, and unexpectedly small projections on those having larger eigenvalues.

6. Conclusions

We have now carried out inverse calculations using TAO data that span almost the full range of tropical Pacific variability (only extreme La Niña conditions have not been represented in the observations), and using an intermediate coupled ocean–atmosphere model very much like the Cane–Zebiak model. Our model included equations of motion, and also our hypothesis $\mathcal{H}_0$ about the errors in those equations. Three anomalous events were involved: an El Niño with a warm pool on the date line (year 1), a La Niña (year 2), and an El Niño with some of the warmest equatorial waters in the historical record (year 3). Our weighted least squares best fit to the model and the data did fit the data to within standard errors, but did not fit the model; the null hypothesis was strongly rejected by a significance test. Had the hypothesis been weakened after year 1 (moderately greater errors), it would not have been rejected after year 2 but would have been strongly rejected after year 3. In any event, the term imbalances in all three years, based on the original hypothesis $\mathcal{H}_0$, showed that the least squares estimates of the circulation have no dynamical credibility. We conclude that the dynamics of El Niño are more complicated than our intermediate model or any simpler model.

The generalized inversion algorithm generates conditioning information that may be interpreted (Bennett 1992, section 6) as the efficiency of the TAO array for observing the hypothetical circulation. However, the actual TAO data led us to reject the hypothesis. Hence the array assessment was unsoundly based and so was not included here. We wish to emphasize that such a risk is inherent in a priori array assessment. Our assessment appears to be a posteriori, because the conditioning information derives from dynamics linearized about $\hat{\mathbf{U}}$, which is the actual inverse or optimal estimate of the circulation. However, one could proceed a priori by linearizing about a composite El Niño, for example. The insensitivity of the conditioning information to the state of linearization (not shown here) supports such a design strategy.

Intermediate coupled models of the tropical Pacific having been rejected by the TAO data, we are now constructing the generalized inverse of a reduced-gravity primitive equation ocean model based closely after Gent and Cane (1989). All numerically resolvable advective processes are included in the model, and vertical resolution of the seasonal thermocline is adequate. The turbulence parameterizations remain a source of uncertainty. Estimating the lowest moments of the errors in these parameterizations is the pressing scientific problem. We shall challenge the model with the five years of TAO data since the completion of the array in 1994.

Correction. Bennett et al. (1998; Part I) p. 1781, column 2, lines 15–16, should read: "... of strength $c_a^2[gH^{(1)}]^{-1}\rho^a KT(\rho_1 C_p)^{-1}$, where C_p is the heat capacity of sea water, is an order of magnitude smaller. . . ."

Acknowledgments. AFB is supported by NSF (9520956-OCE). BC is supported by the NOAA National Centers for Environmental Prediction, through the UCAR Visiting Scientist Program. DEH is supported by NOAA (PMEL, OAR, and OGP) through the UW–NOAA Hayes Center. MJM is supported by the NOAA Office of Global Programs and Environmental Research Laboratories. The CM500e Connection Machines were provided by the Office of Naval Research. The CM5 Connection Machine is supported by NASA EOS and we are grateful to Mark Abbott for access to it. The constructive criticisms of the anonymous reviewers are

acknowledged. Special thanks are owed to Dai McClurg of NOAA/PMEL for preparing the TAO data and to Florence Beyer for typing the manuscript.

APPENDIX

Prior and Posterior Penalties

The following remarkable situation obtained in year 1, year 2, and year 3; the prior penalty was far less than expected ($\mathcal{J}_F \ll E\mathcal{J}_F$), but the posterior penalty exceeded its expected value ($E\hat{\mathcal{J}} < \hat{\mathcal{J}}$) (see Table 3). This is remarkable, because the actual prior penalty indicates that the null hypothesis $\mathcal{H}_0$ is excessively pessimistic, and the actual posterior penalty indicates that $\mathcal{H}_0$ is optimistic. The purpose of this appendix is to reveal how this situation can arise.

Consider first the prior penalty $\mathcal{J}_F$. It consists entirely of data penalty, because the prior or forward model $\mathbf{U}_F$ exactly satisfies the dynamics and the initial conditions $\mathbf{U} = \mathbf{U}_I$. It is immediately clear from (4.6) of B98 that

$$\mathcal{J}_F = \mathbf{h}^{\mathrm{T}}\mathbf{C}_{\epsilon\epsilon}^{-1}\mathbf{h}, \tag{A.1}$$

where $\mathbf{h} = \mathbf{d} - \mathcal{L}[\mathbf{U}_F]$ is the prior data misfit, $\mathbf{d}$ being the data, and $\mathcal{L}$ the M-component vector of linear measurement functionals. Again, $\mathbf{C}_{\epsilon\epsilon}$ is the data error covariance matrix. It may be shown (Bennett 1992, section 5.6) that

$$E\mathbf{h} = 0, \qquad E\mathbf{h}\mathbf{h}^{\mathrm{T}} = \mathbf{P} = \mathbf{R} + \mathbf{C}_{\epsilon\epsilon}, \tag{A.2}$$

where E denotes expectation and $\mathbf{R}$ is the symmetric positive definite "representer matrix." Let the diagonalization of $\mathbf{R}$ be

$$\mathbf{R} = \mathbf{Z}\mathbf{\Lambda}\mathbf{Z}^{\mathrm{T}}, \tag{A.3}$$

where $\mathbf{Z}$ is orthonormal and $\mathbf{\Lambda} = \mathrm{diag}(\lambda_1, \ldots, \lambda_M)$ is diagonal. We may always assume that the eigenvalues are in decreasing order: $\lambda_1 \geq \lambda_2 \geq \cdots \geq \lambda_M > 0$. Let us now assume for simplicity that the data errors are uncorrelated and have the same variance μ^2. Then $\mathbf{R}$, $\mathbf{C}_{\epsilon\epsilon}$, and $\mathbf{P}$ can simultaneously be diagonalized:

$$\mathbf{P} = \mathbf{Z}(\mathbf{\Lambda} + \mu^2\mathbf{I})\mathbf{Z}^{\mathrm{T}}. \tag{A.4}$$

Define the *rotated* prior data misfit $\mathbf{h}'$ as

$$\mathbf{h}' = \mathbf{Z}^{\mathrm{T}}\mathbf{h}. \tag{A.5}$$

Note that

$$E\mathbf{h}' = 0, \qquad E\mathbf{h}'\mathbf{h}'^{\mathrm{T}} = \mathbf{\Lambda} + \mu^2\mathbf{I}. \tag{A.6}$$

Then the prior penalty may be written as

$$\mathcal{J}_F = \mu^{-2}\mathbf{h}'^{\mathrm{T}}\mathbf{h}' \tag{A.7}$$

and its expected value is

$$E\mathcal{J}_F = \mu^{-2}\,\mathrm{Tr}(\mathbf{\Lambda} + \mu^2\mathbf{I}). \tag{A.8}$$

We are interested in the situation

$$\sum_{m=1}^{M} h_m'^2 \ll \sum_{m=1}^{M} (\lambda_m + \mu^2). \tag{A.9}$$

Consider next the posterior penalty $\hat{\mathcal{J}}$. It consists of dynamical penalty, initial penalty, and data penalty. A little algebra (Bennett 1992, section 5.5) shows that

$$\hat{\mathcal{J}} = \mathbf{h}^{\mathrm{T}}\mathbf{P}^{-1}\mathbf{h}. \tag{A.10}$$

In terms of the rotated prior data misfits, this becomes

$$\hat{\mathcal{J}} = \mathbf{h}'^{\mathrm{T}}\mathbf{\Lambda}^{-1}\mathbf{h}', \tag{A.11}$$

with expected value

$$E\hat{\mathcal{J}} = \mathrm{Tr}(\mathbf{\Lambda}^{-1/2}E\mathbf{h}'\mathbf{h}'^{\mathrm{T}}\mathbf{\Lambda}^{-1/2}) = \mathrm{Tr}(\mathbf{I}) = M, \tag{A.12}$$

so we are also interested in the situation

$$M \ll \sum_{m=1}^{M} h_m'^2(\lambda_m + \mu^2)^{-1}. \tag{A.13}$$

Suppose that the array is M_σ-fold redundant:

$$\begin{aligned} 0 < \lambda_M \leq \lambda_{M-1} \leq \cdots \leq \lambda_{M-M_\sigma+1} \\ \ll \mu^2 \ll \lambda_{M-M_\sigma} \leq \cdots \leq \lambda_1. \end{aligned} \tag{A.14}$$

That is, suppose that the expected variances $\lambda_m + \mu^2$ of the projections h_m' of the prior data misfit $\mathbf{h}$ onto the M_σ less stable ($M - M_\sigma$ more stable) of the M orthogonal modes of observability or "array modes" (Bennett 1992, section 6) are the same (far greater than) the data noise level. Assume also that the $M - M_\sigma$ stabler projections are actually far smaller than expected:

$$h_m'^2 \ll \lambda_m + \mu^2 \qquad 1 \leq m \leq M - M_\sigma. \tag{A.15}$$

Then (A.9) and (A.13) may be approximated as

$$M_\sigma\mu^2 \ll \sum_{m=M-M_\sigma+1}^{M} h'^2_m \ll \sum_{m=1}^{M-M_\sigma} \lambda_m. \tag{A.16}$$

That is, the actual variance of the less stable projections is unexpectedly large, but not as large as the expected variance of the more stable projections. This is feasible whenever the array is redundant. The probability of (A.16) could in principle be calculated assuming multivariate normality, but we have not attempted to do so.

REFERENCES

Bennett, A. F., 1992. *Inverse Methods in Physical Oceanography, Monographs on Mechanics and Applied Mathematics.* Cambridge University Press, 346 pp.

——, B. S. Chua, and L. M. Leslie, 1996: Generalized inversion of a global numerical weather prediction model. *Meteor. Atmos. Phys.*, **60,** 165–178.

——, ——, and ——, 1997: Generalized inversion of a global numerical weather prediction model. II: Analysis and implementation. *Meteor. Atmos. Phys.*, **62,** 129–140.

——, ——, D. E. Harrison, and M. J. McPhaden, 1998: Generalized inversion of Tropical Atmosphere–Ocean data and a coupled model of the tropical Pacific. *J. Climate,* **11,** 1768–1792.

Gent, P. R., and M. A. Cane, 1989: A reduced gravity, primitive equation model of the upper equatorial ocean. *J. Comput. Phys.*, **81,** 444–480.

McPhaden, M. J., 1999a: Genesis and evolution of the 1997–98 El Niño. *Science,* **283,** 950–954.

——, 1999b: El Niño: The child prodigy of 1997–98. *Nature,* **398,** 559–562.

Rasmussen, E. M., and T. H. Carpenter, 1982: Variations in tropical sea surface temperature and surface wind fields associated with the Southern Oscillation/El Niño. *Mon. Wea. Rev.*, **110,** 354–384.

Soreide, N. N., D. C. McClurg, W. H. Zhu, M. J. McPhaden, D. W. Denbo, and M. W. Renton, 1996: World Wide Web access to real-time and historical data from the TAO array of moored buoys in the tropical Pacific Ocean: Updates for 1996. *Proc. OCEANS 96*, Fort Lauderdale, FL, MTS/IEEE, 1354–1359.

Talagrand, O., 1972: On the damping of high-frequency motions in four-dimensional assimilation of meteorological data. *J. Atmos. Sci.*, **29,** 1571–1574.

Zebiak, S. E., and M. A. Cane, 1987: A model El Niño–Southern Oscillation. *Mon. Wea. Rev.*, **115,** 2262–2278.